Flux-line-cutting and flux-pinning losses in type-II superconductors in rotating magnetic fields

John R. Clem and Antonio Perez-Gonzalez
Ames Laboratory—U.S. Department of Energy and Department of Physics, Iowa State University, Ames, Iowa 50011
(Received 25 June 1984)

A general critical-state theory, including the effects of both flux-line cutting and flux pinning, is proposed for calculations of hysteresis in type-II superconductors in parallel applied magnetic fields that vary in both magnitude and direction. In this theory, if the magnitude of the electrical-current-density component perpendicular to the magnetic induction $\vec{B}$ exceeds the corresponding critical value $J_{c\perp}$, depinning occurs, and an electric field component $E_\perp$ perpendicular to $\vec{B}$ appears; if the magnitude of the current-density component parallel to $\vec{B}$ exceeds the corresponding critical value $J_{c||}$, flux-line cutting occurs, and an electric field component $E_{||}$ parallel to $\vec{B}$ appears. Model calculations are performed to solve for the electrodynamic response of a slab subjected to a parallel, constant magnetic field whose direction undergoes either continuous rotation or periodic oscillation. The relation of the theory to the pioneering experiments of LeBlanc and co-workers is discussed.

I. INTRODUCTION

The behavior of a type-II superconductor subjected to a parallel magnetic field that slowly rotates relative to the specimen was investigated recently in a series of important experiments by LeBlanc and co-workers.[1–3] To explain the results, fundamental new equations must be added to the existing theory for the static and dynamic magnetic behavior of type-II superconductors. In these experiments a stationary, irreversible type-II superconducting disk was subjected to an applied magnetic field $\vec{H}_0$ parallel to the flat disk faces. Four initial magnetic states of the disk were examined; these were termed[1] nonmagnetic, diamagnetic, paramagnetic, and hybrid, depending upon the magnetic history of the specimen. The nonmagnetic initial state, for example, was produced by cooling the specimen through its transition temperature in the presence of $\vec{H}_0$, such that the initial magnetic flux density $\vec{B}_0 \cong \mu_0 \vec{H}_0$ was nearly uniform. Thus the disk initially contained an array of vortices of nearly constant density $n_0 = B_0/\phi_0$, where $\phi_0 = h/2e = 2.07\times10^{-15}$ T m^2. The disk was then slowly rotated about the axis perpendicular to the flat surfaces, and the two components (parallel and perpendicular to $\vec{H}_0$) of the magnetic flux parallel to the faces were monitored.

Several striking effects occurred in the experiments:[1–3] First, during the initial stages of rotation, the magnitude B of the magnetic flux density in the disk *decreased*, as if vortices somehow were expelled from the specimen against the Lorentz force. Second, as rotation continued, a diamagnetic profile of B versus distance x from the disk's surface (i.e., B decreasing with x) developed in an outer, active region near the disk's faces. Third, as rotation progressed, the diamagnetic profile penetrated inward toward the disk's midplane until B was brought to zero at a distance x_0 from the surface. This effect occurred, however, only when flux pinning was sufficiently strong that $x_0 < X/2$, where X is the disk thickness. Fourth, as rotation proceeded further, the magnetic flux distribution in an inner, trapped-flux region of thickness $X-2x_0$ straddling the disk's midplane, containing vortices pinned within the disk, rotated rigidly along with the disk, while the magnetic flux distribution in the outer, active regions within x_0 of either surface kept a fixed orientation relative to $\vec{H}_0$ and thus moved relative to the disk. The planes on which $B=0$ at a distance x_0 from either surface thus decoupled the vortices in the inner, trapped-flux region, where there was no dissipation, from the outer, active regions, where dissipation occurred.

From the empirical model introduced by the authors of Refs. 1–3, one can show that in the outer, active region both the induced current density $\vec{J}$ and the electric field $\vec{E}$ have components $J_{||}$ and $E_{||}$ parallel to the local magnetic induction $\vec{B}$. The parallel component of $\vec{E}$ cannot be understood using only the familiar expression[4,5] $\vec{E}=\vec{B}\times\vec{v}$, which is believed to hold when $\vec{J}$ has only a component $J_\perp$ perpendicular to $\vec{B}$. (Here, $\vec{v}$ is the vortex velocity.) This component of $\vec{E}$, however, can be understood in terms of flux-line cutting[6,7] (intersection and cross joining of adjacent nonparallel vortices). Recently, it has been shown that for a sufficiently large current density $J_{c||}$ parallel to the vortices or, equivalently, for a sufficiently large vortex angle gradient $k_{c||}$, instabilities of the vortex array[8–14] can occur which lead to flux-line cutting, thereby generating a component[15–17] $E_{||}$ parallel to $\vec{B}$. The parallel components $J_{||}$ and $E_{||}$ together produce a contribution[18] $J_{||}E_{||}$ to the energy dissipation which adds to the familiar flux-flow (flux-pinning) contribution $J_\perp E_\perp$.

In this paper we treat the rotating-magnetic-field problem in type-II superconductors using the theory of flux-line-cutting losses presented in Ref. 18. We shall show that the main results of Refs. 1–3 find a natural explanation in terms of flux-line cutting. In Sec. II we review the key results of Ref. 18 and formulate a general critical-state theory which describes the critical-flux-density pro-

files at the threshold of depinning or flux-line cutting. In the remainder of the paper we consider the behavior of a type-II superconducting slab subjected to a rotating or oscillating parallel applied magnetic field $\vec{H}_s$. The behavior is equivalent to that of a rotating or oscillating slab subjected to a fixed parallel applied magnetic field. In Sec. III we present the final quasi-steady-state solutions achieved when $\vec{H}_s$ rotates with a constant angular velocity, and in Sec. IV we present ac solutions when the angle α_s of $\vec{H}_s$ oscillates with a limited amplitude α_0. Finally, in Sec. V we summarize our findings, point out similarities to and differences from the empirical model of Refs. 1–3, compare our results with those of Bean,[19] and discuss desired extensions of the theory.

II. FORMULATION OF THE GENERAL CRITICAL-STATE THEORY

Consider a high-κ irreversible type-II superconducting infinite slab with surfaces at $x=0$ and $x=X=2x_m$. An external magnetic induction

$$\vec{B}_s(t)=\mu_0\vec{H}_s(t)=B_0\hat{\alpha}_s(t)$$

of fixed magnitude B_0 but time-varying direction,

$$\hat{\alpha}_s=\hat{y}\sin\alpha_s+\hat{z}\cos\alpha_s \ , \tag{1}$$

is applied, inducing fields in the superconductor, $\vec{B}$, $\vec{J}$, and $\vec{E}$, which are parallel to the surfaces and which depend only upon the coordinate x and the time t. For simplicity we assume that, to good approximation, $\vec{B}\approx\mu_0\vec{H}$ over the most important field range, and that the length scales for spatial variation of $\vec{B}$, $\vec{J}$, and $\vec{E}$ are much longer than the weak-field penetration depth λ. We write $\vec{B}=B\hat{\alpha}$, where $B=|\vec{B}|$ and

$$\hat{\alpha}=\hat{y}\sin\alpha+\hat{z}\cos\alpha \ . \tag{2}$$

We assume that the boundary conditions at $x=0$ and $x=X$ and are $B=B_0$ and $\alpha=\alpha_s$; i.e., we neglect the distinction between B and μ_0H in the superconductor and assume no barriers against flux entry or exit at the surface.

From Ampere's law, $\vec{J}=\vec{\nabla}\times\vec{H}$, we obtain $\vec{J}=J_{||}\hat{\alpha}+J_\perp\hat{\beta}$, where

$$\hat{\beta}=\hat{\alpha}\times\hat{x}=\hat{y}\cos\alpha-\hat{z}\sin\alpha \ , \tag{3}$$

$$J_{||}=\mu_0^{-1}B\frac{\partial\alpha}{\partial x} \ , \tag{4}$$

$$J_\perp=-\mu_0^{-1}\frac{\partial B}{\partial x} \ . \tag{5}$$

From Faraday's law, $\vec{\nabla}\times\vec{E}=-\partial\vec{B}/\partial t$, we obtain $\vec{E}=E_{||}\hat{\alpha}+E_\perp\hat{\beta}$, where

$$\frac{\partial E_{||}}{\partial x}=B\frac{\partial\alpha}{\partial t}+E_\perp\frac{\partial\alpha}{\partial x} \ , \tag{6}$$

$$\frac{\partial E_\perp}{\partial x}=-\frac{\partial B}{\partial t}-E_{||}\frac{\partial\alpha}{\partial x} \ . \tag{7}$$

As pointed out in Ref. 18, combining Eqs. (4) and (7) yields

$$\frac{\partial B}{\partial t}+\frac{\partial j_{Bx}}{\partial x}=-\mu_0J_{||}E_{||}/B \ , \tag{8}$$

where

$$j_{Bx}=E_\perp=Bv_x \tag{9}$$

is the B-current density. Equation (8) shows that a region of space in which flux-line cutting is occurring ($J_{||}E_{||}>0$) serves as a sink for B; in other words, *flux-line cutting consumes B.*

For slow variation of α_s, such that eddy currents are negligible, local vortex configurations generating the flux density $\vec{B}$ are assumed to be governed by the following general critical-state principles: Metastable stationary distributions of $\vec{B}$, in which $E_\perp=0$, are always such that the magnitude of $J_\perp$ obeys

$$|J_\perp|\le J_{c\perp}(B) \ , \tag{10}$$

where $J_{c\perp}(B)>0$ is the function describing the transverse critical-current density at the threshold for the depinning of a vortex array from a distribution of bulk pinning centers in the specimen. This condition is equivalent to the statement that the magnitude of the Lorentz force, $F_{Lx}=J_\perp B$, never exceeds the volume-pinning force $F_p(B)\equiv J_{c\perp}(B)B$. Similarly, metastable distributions of α, in which $E_{||}=0$, are always such that the magnitude of $J_{||}$ obeys

$$|J_{||}|\le J_{c||}(B) \ , \tag{11}$$

where $J_{c||}(B)>0$ is the function describing the longitudinal critical-current density at the threshold for the onset of flux-line cutting in the vortex array.[18] Using Eq. (4), we can reexpress Eq. (11) as

$$\left|\frac{\partial\alpha}{\partial x}\right|\le k_{c||}(B) \ , \tag{12}$$

where

$$k_{c||}(B)=\mu_0J_{c||}(B)/B \ . \tag{13}$$

Throughout this paper we assume isothermal behavior and ignore the temperature dependence of $J_{c\perp}$, F_p, $J_{c||}$, and $k_{c||}$.

Flux redistribution occurs when $J_\perp$ exceeds $J_{c\perp}$, in which case $E_\perp>0$ and $J_\perp E_\perp>0$; when $J_\perp<-J_{c\perp}$, we have $E_\perp<0$, such that again $J_\perp E_\perp>0$. Flux distribution also occurs when $J_{||}$ exceeds $J_{c||}$, in which case $E_{||}>0$ and $J_{||}E_{||}>0$; when $J_{||}<-J_{c||}$ we have $E_{||}<0$, such that again $J_{||}E_{||}>0$. Regardless of their spatial dependences, both $E_\perp$ and $E_{||}$ are continuous functions of x. We denote a zone in which (a) only flux transport occurs ($E_\perp\neq0$ but $E_{||}=0$) as a T zone, (b) only flux cutting occurs ($E_{||}\neq0$ but $E_\perp=0$) as a C zone, (c) both flux cutting and transport occur ($E_{||}\neq0$ and $E_\perp\neq0$) as a CT zone, and (d) neither flux cutting nor transport occurs ($E_{||}=0$ and $E_\perp=0$) as an O zone. In addition, we use subscripts $+$ and $-$ to indicate the signs of $E_\perp$ or $E_{||}$. For example, a T_+ zone is one in which $E_\perp>0$ but $E_{||}=0$, and a C_-T_+ zone is a zone in which $E_{||}<0$ and $E_\perp>0$.

Equations (1)–(13) are concise statements of the general

critical-state theory (incorporating both flux pinning and flux-line cutting) to be used in this paper. We now show how these equations can be applied to calculate the distributions of $\vec{B}$, $\vec{J}$, and $\vec{E}$ as well as energy dissipation, for a variety of cases. To bring out the physics with the least mathematical complication, we take $J_{c\perp}$ and $k_{c\|}$ to be constants independent of B. To obtain detailed agreement with experiment, however, it would be necessary to take into account the dependences of $J_{c\perp}$ and $k_{c\|}$ upon B. For the calculations of Secs. III—V the profiles of B and α obey

$$\frac{\partial B}{\partial x}=\pm B_0/x_0 \tag{14}$$

at the threshold of depinning, and

$$\frac{\partial \alpha}{\partial x}=\pm k_{c\|} \tag{15}$$

at the threshold of flux cutting, where $x_0=B_0/\mu_0 J_{c\perp}$ is the distance from the surface at which B would be reduced from B_0 to zero along a diamagnetic profile. It also is convenient to introduce the ratio of $J_{c\|}$ at B_0 to $J_{c\perp}$,

$$\chi=k_{c\|}x_0=J_{c\|}(B_0)/J_{c\perp}\ . \tag{16}$$

Interpretation of the experiments of Refs. 1—3 in terms of Eqs. (14)—(16) suggests that, for the specimens studied, $\chi\sim 10$ for large B, that $\chi>1$ for most of the field range investigated, and that $\chi<1$ only for very small B_0. For the conditions considered in this paper there is symmetry about the midplane $x=x_m=X/2$ of the slab, such that $\vec{B}(x,t)=\vec{B}(X-x,t)$. We thus examine the distributions of $\vec{B}$, $\vec{J}$, and $\vec{E}$ only in the region $0\le x\le x_m$.

III. QUASI-STEADY-STATE SOLUTIONS

We consider first the solutions for $\vec{B}$, $\vec{J}$, and $\vec{E}$ achieved in quasi steady state after a long time of slow rotation, such that the surface field angle $\alpha_s=\omega t$ obeys $\alpha_s\gg 1$. Although the macroscopic electric field $\vec{E}$ here is time independent, the term quasi steady state is appropriate because $\vec{E}$ is produced on a microscopic scale by generally very complicated motions of vortices or vortex segments: $E_\perp$ is generated by translational vortex motion and $E_\|$ by countermotion of adjacent vortex segments.[18] According to Eq. (8), flux-line cutting during the initial stages of rotation consumes B within the slab, such that, regardless of the slab's initial magnetic state, $B(x)\approx B_0(1-x/x_0)$ and $J_\perp\approx J_{c\perp}$ wherever dissipation occurs in steady state. The dissipative region extends to the slab's midplane ($x=x_m=X/2$) if $x_0>x_m$, but only as far as $x=x_0=B_0/\mu_0 J_{c\perp}$ if $x_0<x_m$. Within the dissipative region, $\partial\alpha/\partial t=\omega$.

The details of the quasi-steady-state solutions depend upon the particular values of $\chi=k_{c\|}x_0=J_{c\|}(B_0)/J_{c\perp}$ and $\mu=k_{c\|}x_m$. When χ and μ lie in region A of Fig. 1, i.e., when $\mu>\chi$, dissipation is limited to an outer, active, CT zone, $0\le x<x_0$, in which both flux-line cutting and transport occur. The magnetic flux distribution remains stationary in an inner, trapped-flux, O zone, $x_0\le x\le x_m$, in which neither flux-line cutting nor transport occurs; the values of B and α in this zone depend upon the initial magnetic state. In regions B and C of Fig. 1, where $\mu<\chi$, dissipation occurs throughout the entire region $0\le x<x_m$. Regions B and C are separated by the curve $\mu=\mu_1(\chi)$, where

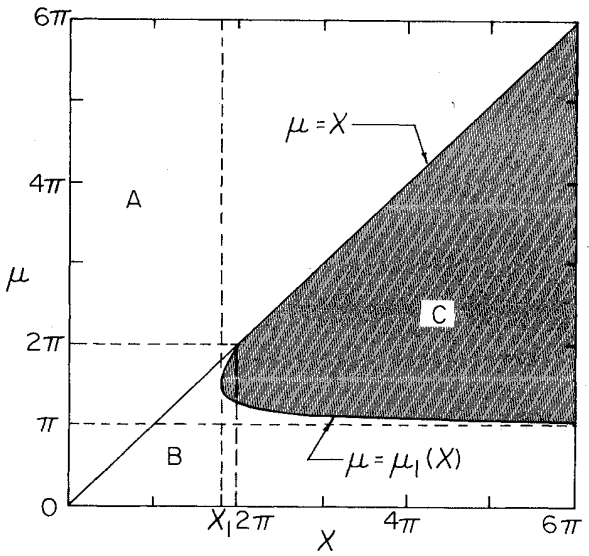

FIG. 1. Dissipation during constant rotation (a) is confined to within x_0 of either surface in region A, (b) occurs throughout the slab of thickness $X=2x_m$ in regions B and C, and (c) is unstable in region C (cross-hatched). Here, $\mu=k_{c\|}x_m$ and $\chi=k_{c\|}x_0$.

$$\mu_1=\chi-\cot(\mu_1/2-\pi/2),\quad \pi<\mu_1\le 2\pi\ . \tag{17}$$

The curve of μ_1 versus χ has infinite slope at $\chi_1=1+3\pi/2=5.71$, where $\mu_1(\chi_1)=3\pi/2$. In region B of Fig. 1, both flux-line cutting and transport occur continuously throughout the region $0\le x<x_m$, a CT zone. In the cross-hatched region C of Fig. 1, time-dependent instabilities, similar to flux jumps, are predicted to occur. The resulting electromagnetic behavior can be described in terms of moving T and CT zones, but is too complex to discuss in detail in this paper.

A. Region A

For values of χ and μ in region A of Fig. 1,

$$\alpha(x,t)=\omega t-k_{c\|}x$$

and

$$J_\|(x)=-(B_0k_{c\|}/\mu_0)(1-x/x_0)\ .$$

The solutions of Eqs. (6) and (7), subject to $E_\|(x_0)=E_\perp(x_0)=0$, are

$$E_\|(x)=-(\omega B_0/k_{c\|}\chi)\{1-\cos[k_{c\|}(x_0-x)]\}\ , \tag{18}$$

$$E_\perp(x)=(\omega B_0/k_{c\|})\{(1-x/x_0)-\chi^{-1}\sin[k_{c\|}(x_0-x)]\}\ . \tag{19}$$

Throughout the C_-T_+ zone, $0\le x<x_0$, $E_\|\le 0$ and $E_\perp>0$, even for large values of the arguments of the sine and cosine. This must be true in order to have both

$J_{||}E_{||} \geq 0$ and $J_\perp E_\perp > 0$, since $J_{||} < 0$ and $J_\perp > 0$. Figure 2(a) shows a plot of $E_\perp$ (solid line) and $E_{||}$ (dashed line), in units of $\omega B_0/k_{c||}$, versus x for $\chi = 8$.

Because $\partial B/\partial t = 0$, Poynting's theorem[20] states that the rate of energy dissipation per unit surface area is equal to the x component of the Poynting vector at $x = 0$,

$$S_x(0) = E_\perp(0)B_0/\mu_0 = [\omega B_0^3/\mu_0^2 J_{c||}(B_0)](1-\chi^{-1}\sin\chi) . \quad (20)$$

B. Region *B*

For values of χ and μ in region B of Fig. 1, $\alpha(x,t) = \omega t - k_{c||}x$ and $J_{||}(x) = -(B_0 k_{c||}/\mu_0)(1-x/x_0)$. The solutions of Eqs. (6) and (7), subject to $E_{||}(x_m) = E_\perp(x_m) = 0$, are

$$E_{||}(x) = -(\omega B_0/k_{c||})((1-x_m/x_0)\sin[k_{c||}(x_m-x)] + \chi^{-1}\{1-\cos[k_{c||}(x_m-x)]\}) , \quad (21)$$

$$E_\perp(x) = (\omega B_0/k_{c||})\{(1-x/x_0) - (1-x_m/x_0)\cos[k_{c||}(x_m-x)] - \chi^{-1}\sin[k_{c||}(x_m-x)]\} . \quad (22)$$

Throughout the C_-T_+ zone, $0 \leq x < x_m$, $E_{||} < 0$ and $E_\perp > 0$. Figure 2(b) shows a plot of $E_\perp$ (solid line) and $E_{||}$ (dashed line), in units of $\omega B_0/k_{c||}$, versus x for $\chi = 8$ and for three values of μ: 2, 3.6[$\mu_1(8)$], and 6. Note that, when $\mu = 2$, $E_{||} \leq 0$ and $E_\perp \geq 0$ for all x, but when $\mu = \mu_1(8) = 3.6$, which is at the boundary of the unstable region C of Fig. 1, $E_{||}(0) = 0$ at the surface. When $\mu = 6$ [in region C: $\mu_1(x) < \mu < \chi$], Eq. (21) yields positive values of $E_{||}$ (dotted line) and negative values of $J_{||}E_{||}$ near the surface. This is unphysical, since $J_{||}E_{||}$, the flux-line-cutting contribution to the dissipation, must obey $J_{||}E_{||} \geq 0$. This behavior therefore indicates that the assumptions leading to Eqs. (21) and (22), while valid in region B of Fig. 1, are *invalid* for μ and χ in region C. Numerical solutions confirm this and, in addition, show that complicated instabilities can occur in region C.

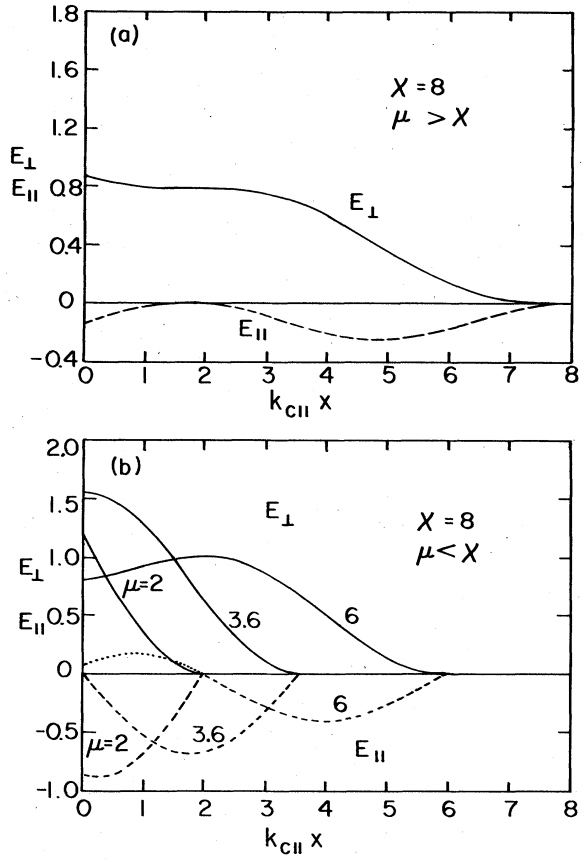

FIG. 2. (a) $E_\perp$ (solid line) and $E_{||}$ (dashed line) [Eqs. (19) and (18)], in units of $\omega B_0/k_{c||}$, versus x for χ and μ in region A of Fig. 1. Here, $\chi = k_{c||}x_0 = 8$ and $\mu = k_{c||}x_m > \chi$. (b) $E_\perp$ (solid line) and $E_{||}$ (dashed line) [Eqs. (22) and (21)], in units of $\omega B_0/k_{c||}$, versus x for χ and μ in regions B and C of Fig. 1. Curves are shown for $\chi = k_{c||}x_0 = 8$ and for three values of $\mu = k_{c||}x_m$: (i) 2 (region B), (ii) $\mu_1(8) = 3.6$ (boundary between regions B and C), and (iii) 6 (region C). The dotted portion of $E_{||}$ versus x for $\mu = 8$ is unphysical, indicating that Eqs. (21) and (22) do not apply in region C.

For μ and χ in region B the rate of energy dissipation per unit surface area, obtained by Poynting's theorem, is

$$S_x(0) = [\omega B_0^3/\mu_0^2 J_{c||}(B_0)] \times [1-\cos\mu - \chi^{-1}(\sin\mu - \mu\cos\mu)] . \quad (23)$$

The expressions for $S_x(0)$ in regions A and B [Eqs. (20) and (23)] coincide along the boundary $\mu = \chi$ in Fig. 1, where both $S_x(0)$ and its first derivative with respect to μ (or χ) are continuous functions of χ and μ. For thin ($\mu \ll 1$) slabs, $S_x(0) \propto \mu^2$, and for thick ($\mu > \chi$) slabs, $S_x(0)$ is independent of μ [Eq. (20)]. For $\chi \leq \pi$, $S_x(0)$ is a monotonically increasing function of μ, but for $\chi > \pi$, Eq. (23) predicts that $S_x(0)$ has a maximum at $\mu = \pi$, where

$$S_x^{\max}(0) = [\omega B_0^3/\mu_0^2 J_{c||}(B_0)](2-\pi/\chi) . \quad (24)$$

The behavior of $S_x(0)$ versus μ for various values of χ is shown in Fig. 3. Portions of the curves corresponding to values of χ and μ in region B of Fig. 1 are indicated by solid curves, and those portions in region A, by dashed lines. When $\chi > 5.71$, the solid curves end at $\mu = \mu_1(\chi)$ [Eq. (17)], where the region of instability C begins.

In all cases the rate of energy dissipation per unit volume $\vec{J}\cdot\vec{E}$ is the sum of the flux-pinning contribution $J_\perp E_\perp$ and the flux-line-cutting contribution $J_{||}E_{||}$, both of which are non-negative. The integral of $\vec{J}\cdot\vec{E}$ from $x = 0$ to the smaller of x_0 and x_m is equal to $S_x(0)$. Referring to Eq. (8), we identify $\mu_0 J_{||}E_{||}/B = -k_{c||}E_{||}$ in each case as the rate at which flux-line cutting locally consumes B and $\partial j_{Bx}/\partial x = \partial E_\perp/\partial x$ as the rate at which flux transport replenishes B. These two rates are equal in quasi steady state, such that $\partial B/\partial t = 0$.

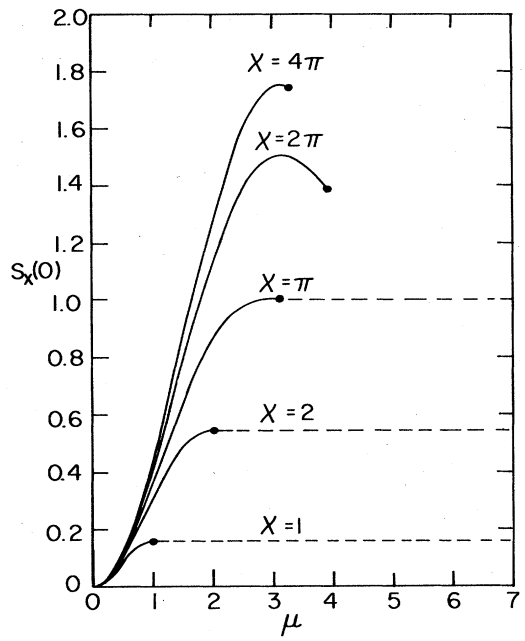

FIG. 3. $S_x(0)$ in units of $\omega B_0^3/\mu_0^2 J_{c\|}(B_0)$ versus $\mu = k_{c\|} x_m$ for several values of $\chi = k_{c\|} x_0$. Solid curves [Eq. (23)] correspond to region B of Fig. 1; dashed lines [Eq. (20)], region A; for $\chi > 5.71$, solid curves end at $\mu = \mu_1(\chi)$, the boundary between regions B and C.

IV. ac SOLUTIONS

We consider next the solutions for $\vec{B}$, $\vec{J}$, and $\vec{E}$ achieved under ac conditions for which $\alpha_s(t)$ oscillates with amplitude α_0. We assume that the frequency is sufficiently low that the induced eddy currents make a negligible contribution to the dissipation. The resulting ac losses are then entirely hysteretic and independent of the particular waveform of $\alpha_s(t)$ versus t; e.g., sinusoidal, triangular, and trapezoidal waveforms all yield the same loss per cycle.

As α_s sweeps through its cycle, the details of the time evolution of $\alpha(x,t)$, $E_{\|}(x,t)$, and $E_{\perp}(x,t)$ depend upon three parameters: α_0, $\chi = k_{c\|} x_0$, and $\mu = k_{c\|} x_m$. The behavior is most complex when all three are much larger than unity. For example, when $\alpha_0 \gg 1$ and $\chi < 5.71$ or $\mu < \mu_1(\chi)$, the behavior of $\alpha(x,t)$, $E_{\|}(x,t)$, and $E_{\perp}(x,t)$ is given over most of the cycle by the steady-state results of Sec. III, and the energy dissipation per unit surface area per cycle can be obtained from time integrals of Eqs. (20) and (23). For $\alpha_0 \gg 1$, $\chi > 5.71$, and $\mu > \mu_1(\chi)$ (see Fig. 1), instabilities are expected to occur. Space does not permit a description of the ac losses for all possible combinations of values of α_0, χ, and μ. Instead, we confine our attention to the case for which at least one of these three parameters is sufficiently small so that there is dissipation only in a single zone where both flux-line cutting and flux transport occur. The particular conditions for such single-dissipative-zone behavior are $\chi < \chi_1 = 1 + 3\pi/2 = 5.71$, or, when $\chi \geq \chi_1$, $\min(\alpha_0, \mu) \leq \mu_1(\chi)$ [Eq. (17)], where $\min(\alpha_0, \mu)$ denotes the smaller of α_0 and μ. Referring to Fig. 1 with the ordinate representing either μ or α_0, we see that single-dissipative-zone behavior occur either in regions A and B to the left of the line $\chi = \chi_1$, or in region B under the curve $\mu = \mu_1(\chi)$ or $\alpha_0 = \mu_1(\chi)$.

In the single-dissipative-zone case, dissipation occurs only within a distance $x_c = \alpha_0 / k_{c\|}$ of the surface when $x_c < x_d = \min(x_0, x_m)$, or within a distance x_d of the surface when $x_c > x_d$, i.e., the dissipation occurs within a distance $x_{cd} = \min(x_c, x_d)$ of the surface. The electrodynamic behavior becomes cyclic only after α_s undergoes a certain number of oscillations, the precise number depending upon the specimen's magnetic history. During these preliminary oscillations, flux-line cutting consumes B and ultimately produces the time-independent profile $B(x) = B_0(1 - x/x_0)$ in the dissipative zone $0 \leq x < x_{cd}$. Profiles of $\alpha(x,t)$ versus x are sketched in Fig. 4 for $x_c < x_d$. For $x_d < x_c$ the time-varying portions of $\alpha(x,t)$ versus x are the same, except that they are truncated at $x = x_d$. The two extremal profiles, $\alpha_{\max}(x)$ and $\alpha_{\min}(x)$, correspond to the cases when $\alpha_s = \alpha_0$ and $-\alpha_0$, respectively,

$$\alpha_{\max}(x) = \alpha_0 - k_{c\|} x \ , \tag{25}$$

$$\alpha_{\min}(x) = -\alpha_0 + k_{c\|} x \ . \tag{26}$$

The profile $\alpha_{\uparrow}(x,t)$ corresponds to the case when α_s is increasing.[21] In the region $0 \leq x \leq x_{\uparrow}(t)$, where

$$x_{\uparrow}(t) = [\alpha_0 + \alpha_s(t)]/2k_{c\|} \ , \tag{27}$$

$\alpha(x,t)$ is altered from $\alpha_{\min}(x)$ to

$$\alpha_{\uparrow}(x,t) = \alpha_s(t) - k_{c\|} x \ . \tag{28}$$

At $x = x_{\uparrow}(t)$,

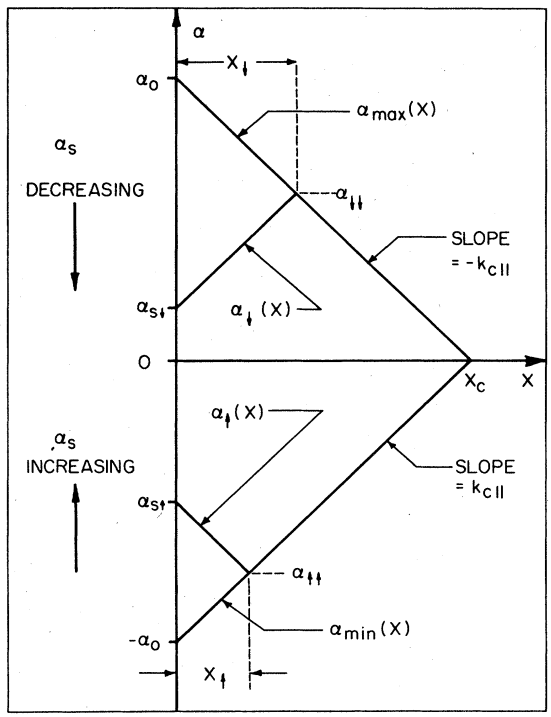

FIG. 4. Sketch of the external field angle profiles $\alpha_{\max}$ and $\alpha_{\min}$, and the α_s-increasing and α_s-decreasing profiles $\alpha_{\uparrow}$ and $\alpha_{\downarrow}$, versus x, calculated from the equation $\partial\alpha/\partial x = \pm k_{c\|}$.

$$\alpha_{\uparrow}(x_{\uparrow},t)=\alpha_{\uparrow\uparrow}(t)=[\alpha_s(t)-\alpha_0]/2\ . \tag{29}$$

It is convenient to define

$$\gamma(t)=[\alpha_0+\alpha_s(t)]/2\ , \tag{30}$$

so that $\gamma=0$ at the beginning and $\gamma=\alpha_0$ at the end of the α_s-increasing half-cycle. The profile $\alpha_{\downarrow}(x,t)$ shown in Fig. 4 corresponds to the case when α_s is decreasing.[18,21] When $x_d<x_c$, Eqs. (26)–(30) still apply, but then we need only the values of $\alpha_{\uparrow}(x,t)$ and $\alpha_{\downarrow}(x,t)$ for $0\le x\le x_d$.

For the α_s-increasing case, $\vec{B}_{\uparrow}(x,t)$, $\vec{J}_{\uparrow}(x,t)$, and $\vec{E}_{\uparrow}(x,t)$ are determined as follows. First, $\vec{B}_{\uparrow}(x,t)=B(x)\hat{\alpha}_{\uparrow}(x,t)$, where $B(x)=B_0(1-x/x_0)$ and

$$\hat{\alpha}_{\uparrow}(x,t)=\hat{y}\sin\alpha_{\uparrow}(x,t)+\hat{z}\cos\alpha_{\uparrow}(x,t)\ . \tag{31}$$

At time t, dissipation occurs only in the region $0\le x<x_{\uparrow d}(t)$, where $x_{\uparrow d}(t)=\min[x_{\uparrow}(t),x_d]$. In this region, $J_{\uparrow||}(x,t)=-k_{c||}B(x)/\mu_0$, $J_{\uparrow\perp}(x,t)=J_{c\perp}=B_0/\mu_0x_0$, and the solutions of Eqs. (6) and (7), subject to $E_{\uparrow\perp}(x_{\uparrow d},t)=E_{\uparrow||}(x_{\uparrow d},t)=0$, are

$$E_{\uparrow||}(x,t)=-(\dot{\alpha}_sB_0/k_{c||})((1-x_{\uparrow d}/x_0)\sin[k_{c||}(x_{\uparrow d}-x)]+\chi^{-1}\{1-\cos[k_{c||}(x_{\uparrow d}-x)]\})\ , \tag{32}$$

$$E_{\uparrow\perp}(x,t)=(\dot{\alpha}_sB_0/k_{c||})\{(1-x/x_0)-(1-x_{\uparrow d}/x_0)\cos[k_{c||}(x_{\uparrow d}-x)]-\chi^{-1}\sin[k_{c||}(x_{\uparrow d}-x)]\}\ , \tag{33}$$

where $\dot{\alpha}_s=d\alpha_s/dt$. When $\chi<\chi_1=1+3\pi/2=5.71$, or, when $\chi>\chi_1$, $\min(\alpha_0,\mu)\le\mu_1(\chi)$, we have $E_{\uparrow||}(x,t)\le0$ and $E_{\uparrow,\perp}(x,t)\ge0$ throughout the region $0\le x\le x_{\uparrow d}(t)$.

The rate of energy dissipation per unit surface area is

$$\begin{aligned}S_{\uparrow x}(0,t)&=E_{\uparrow\perp}(0,t)B_0/\mu_0\\&=(\dot{\alpha}_sB_0^2/\mu_0k_{c||})[1-(1-x_{\uparrow d}/x_0)\cos(k_{c||}x_{\uparrow d})-\chi^{-1}\sin(k_{c||}x_{\uparrow d})]\ .\end{aligned} \tag{34}$$

The time integral of $S_{\uparrow x}(0,t)$ over the α_s-increasing half-cycle yields $W'_{a\uparrow}$, the energy dissipated per unit surface area during this half-cycle. For integration it is helpful to change variables from t to γ, such that $k_{c||}x_{\uparrow d}=\gamma$ when $\gamma\le\alpha_d$, where $\alpha_d=k_{c||}x_d=\min(\chi,\mu)$, and $k_{c||}x_{\uparrow d}=\alpha_d$ when $\alpha_d\le\gamma\le\alpha_0$. A similar calculation for the α_s-decreasing half-cycle yields the corresponding dissipation $W'_{a\downarrow}$, which, by symmetry, is exactly equal to $W'_{a\uparrow}$. The sum of $W'_{a\uparrow}$ and $W'_{a\downarrow}$ is thus the total energy dissipated per unit surface area per cycle,

$$W'_a=[4B_0^3/\mu_0^2J_{c||}(B_0)]\{\alpha_0-\sin\alpha_0-4\chi^{-1}\sin(\alpha_0/2)[\sin(\alpha_0/2)-(\alpha_0/2)\cos(\alpha_0/2)]\} \tag{35a}$$

when $\alpha_0<\alpha_d$, and

$$\begin{aligned}W'_a=[4B_0^3/\mu_0^2J_{c||}(B_0)]\{&\alpha_d-\sin\alpha_d-4\chi^{-1}\sin(\alpha_d/2)[\sin(\alpha_d/2)-(\alpha_d/2)\cos(\alpha_d/2)]\\&+(\alpha_0-\alpha_d)[1-\cos\alpha_d-\chi^{-1}(\sin\alpha_d-\alpha_d\cos\alpha_d)]\}\end{aligned} \tag{35b}$$

when $\alpha_0\ge\alpha_d$. Equation (35a) describes the dissipation when the angle amplitude α_0 is too small to drive the dissipative flux-line-cutting region of thickness $x_c=\alpha_0/k_{c||}$ as deep as either x_0 or the slab's midplane x_m. Equation (35b) applies for larger amplitudes when the thickness of the dissipative region is the smaller of x_0 and x_m.

When $\alpha_0\ll1$ and $\alpha_0<\min(\chi,\mu)$, Eq. (35a) yields, to good approximation,[18]

$$W'_a=\frac{2b_{0\perp}^3}{3\mu_0^2J_{c||}(B_0)}\left[1-\frac{J_{c\perp}}{2J_{c||}(B_0)}\frac{b_{0\perp}}{B_0}\right]\ , \tag{36}$$

where $b_{0\perp}=B_0\sin\alpha_0\cong B_0\alpha_0$ can be regarded as the transverse component (perpendicular to $\vec{B}_0=B_0\hat{z}$) of an applied ac magnetic induction.

V. SUMMARY AND CONCLUSIONS

In this paper we formulated (Sec. II) a general critical-state theory for the hysteretic electrodynamic behavior of a type-II superconducting slab subjected to a parallel magnetic field that changes in both magnitude and direction. Two fundamental material-dependent quantities play key roles in this theory: $J_{c\perp}$, the transverse critical-current density at the threshold of depinning, and $J_{c||}=Bk_{c||}/\mu_0$, the longitudinal critical-current density at the threshold of flux-line cutting. We applied the theory, assuming constant $J_{c\perp}$ and $k_{c||}$ for simplicity, to calculate $\vec{B}$, $\vec{J}$, and $\vec{E}$ and the corresponding energy dissipation in a slab subjected to a parallel, constant magnetic field whose direction undergoes either continuous rotation (Sec. III) or periodic oscillation (Sec. IV).

The theory described in this paper has several similarities to the simple model that was proposed to explain the pioneering experiments of Refs. 1–3. These include (a) the assumption that the steepest metastable gradients of B are governed by $|dB/dx|=\mu_0J_{c\perp}$, regardless of whether the direction of B changes or not, (b) the assumption that the steepest metastable gradients of the angle of $\vec{B}$ are governed by an additional equation, $|d\alpha/dx|=k_{c||}$, and (c) the assertion that rotation ultimately leads to diamagnetic profiles of B near the surface, such that B decreases with distance from the surface according to $|dB/dx|=\mu_0J_{c\perp}$. The present theory, moreover, goes beyond that of Refs. 1–3 by identifying flux-line cutting as the physical mechanism that produces the diamagnetic B profiles near the surface. Faraday's law, when reexpressed as Eq. (8), shows that[18] B is not conserved when flux-line cutting occurs, but instead is irreversibly consumed. Such *B consumption* occurs even though fluxoid conservation is rigorously obeyed during each and every

flux-line-cutting event.[9] The authors of Refs. 1–3, who discovered that rotation reduces B inside a disk initially in a nonmagnetic or paramagnetic state, described[1] this surprising effect as a "flux expulsion" phenomenon, by which "flux can leave this disk although the magnetic pressure is directed inward at the surfaces." With the aid of the present theory, we see that "flux expulsion" is a misleading description of rotation-induced B consumption, because, rather than being transported *out* of the specimen as a result of rotation, vortices near the surface actually undergo net transport *into* the specimen, thereby replenishing B in those regions where flux-line cutting consumes it. We discussed this effect briefly at the end of Sec. III; we plan to provide a more complete description in a subsequent publication including an analysis of the approach to steady state.

Although our theory yields results essentially identical to those of Refs. 1–3 in the quasi steady state and under ac conditions after the diamagnetic profile at the surface has been established, it requires a significantly different description of the time evolution of the profiles of B and α, starting from nonmagnetic and paramagnetic initial states. In the context of our theory, the evolving profiles of B and α proposed in Refs. 1–3, in fact, do not obey Faraday's law [Eqs. (6) and (7)] with continuous $E_\perp$ and $E_\parallel$. In a subsequent publication we plan to show how our theory yields the appropriate B and α profiles, which are, in general, considerably more complex than those of Refs. 1–3.

To compare our results with those of Bean,[19] we first consider the solutions of Eqs. (1)–(13) using the model $J_{c\perp}=\text{const}$ and $J_{c\parallel}=\text{const}=\chi J_{c\perp}$. We assume that $\alpha_s=-\omega t$ and $x_0<x_m$. The results for $0\le x\le x_0=B_0/\mu_0 J_{c\perp}$ are

$$B=B_0(1-x/x_0)\,, \tag{37}$$

$$\alpha=-\omega t-\chi\ln(1-x/x_0)\,, \tag{38}$$

$$E_\perp=\omega B^2/\mu_0 J_{c\parallel}(1+4/\chi^2)\,, \tag{39}$$

$$E_\parallel=2\omega B^2/\mu_0 J_{c\parallel}\chi(1+4/\chi^2)\,. \tag{40}$$

The Poynting vector at the surface is

$$S_x(0)=\omega B_0^3/\mu_0^2 J_{c\parallel}(1+4/\chi^2)\,, \tag{41}$$

and the loss per revolution per unit surface area is

$$W_a'=2\pi B_0^3/\mu_0^2 J_{c\parallel}(1+4/\chi^2)\,. \tag{42}$$

With these assumptions for the B dependence of $J_{c\perp}$ and $J_{c\parallel}$, the angle between $\vec{J}$ and $\vec{B}$ is $\tan^{-1}(1/\chi)$, and the angle between $\vec{E}$ and $\vec{B}$ is $\tan^{-1}(\chi/2)$.

Bean[19] made two restrictive assumptions: (a) $\vec{E}$ always points along $\vec{J}$, and (b) the magnitude of $\vec{J}$ is J_c, the depinning critical-current density. Assumption (a) leads to the condition $1/\chi=\chi/2$ or $\chi=\sqrt{2}$, and assumption (b) leads further to the conditions $J_{c\parallel}=J_c\sqrt{2}/\sqrt{3}$ and $J_{c\perp}=J_c/\sqrt{3}$. Substitution of these into Eq. (42) leads to Bean's result[19] (reexpressed in MKS units):

$$W_a'=2\pi B_0^3/\mu_0^2 J_c\sqrt{6}\,. \tag{43}$$

In our more general theory, assumptions (a) and (b) are replaced by two other assumptions: (a) $J_{c\perp}$ is equal to the usual depinning critical-current density J_c measured by conventional means, and (b) $J_{c\parallel}$ is a new, fundamental, sample-dependent, longitudinal critical-current density at the threshold of flux-line cutting which must be measured or calculated independently of $J_{c\perp}$.

As in the case of the usual critical-state model (including only pinning), simple analytic solutions for the field profiles are obtainable only with simple B dependences of $J_{c\parallel}$ and $J_{c\perp}$. In this paper we have kept these dependences as simple as possible to calculate and illustrate the electrodynamic behavior for a variety of cases. To make detailed comparisons with experiments, such as those in Refs. 1–3, the present theory must be extended to account for the B dependence of both $J_{c\parallel}$ and $J_{c\perp}$, as well as for general time variation of the applied magnetic field $\vec{B}_a$. To this end we have developed a computer program which numerically solves Eqs. (4)–(7) not only for the arbitrary B dependence of $J_{c\parallel}$ and $J_{c\perp}$, but also for arbitrary trajectories of $\vec{B}_a(0,t)$ and $\vec{B}_a(X,t)$. We plan to present our results in a subsequent publication.

ACKNOWLEDGMENTS

We are grateful to Dr. M. A. R. LeBlanc for stimulating discussions and correspondence. Ames Laboratory is operated for the U.S. Department of Energy by Iowa State University under Contract No. W-7405-Eng-82. This work was supported by the Director for Energy Research, Office of Basic Energy Sciences, U.S. Department of Energy.

[1] R. Boyer and M. A. R. LeBlanc, Solid State Commun. **24**, 261 (1977).
[2] R. Boyer, G. Fillion, and M. A. R. LeBlanc, J. Appl. Phys. **51**, 1692 (1980).
[3] J. R. Cave and M. A. R. LeBlanc, J. Appl. Phys. **53**, 1631 (1982).
[4] B. D. Josephson, Phys. Lett. **16**, 242 (1965).
[5] Y. B. Kim and M. J. Stephen, in *Superconductivity,* edited by R. D. Parks (Dekker, New York, 1969), Vol. 2, p. 1133.
[6] D. G. Walmsley, J. Phys. F **2**, 510 (1972).
[7] A. M. Campbell and J. E. Evetts, Adv. Phys. **21**, 199 (1972).
[8] J. R. Clem, Phys. Rev. Lett. **38**, 1425 (1977).
[9] J. R. Clem and S. Yeh, J. Low Temp. Phys. **39**, 173 (1980).
[10] E. H. Brandt, J. Low Temp. Phys. Lett. **79A**, 207 (1980).
[11] E. H. Brandt, J. Low Temp. Phys. **42**, 557 (1981).
[12] E. H. Brandt, J. Low Temp. Phys. **44**, 33 (1981).
[13] E. H. Brandt, J. Low Temp. Phys. **44**, 59 (1981).
[14] E. H. Brandt, Physica (Utrecht) **107B**, 459 (1981).
[15] J. R. Clem, J. Low Temp. Phys. **38**, 353 (1980).
[16] E. H. Brandt, J. Low Temp. Phys. **39**, 41 (1980).
[17] J. R. Clem, Physica (Utrecht) **107B**, 453 (1981).
[18] J. R. Clem, Phys. Rev. B **26**, 2463 (1982).
[19] C. P. Bean, J. Appl. Phys. **41**, 2482 (1970).
[20] J. D. Jackson, *Classical Electrodynamics* (Wiley, New York, 1962), p. 189.
[21] The subscripts ↑ and ↓ refer to the α_s-increasing and α_s-decreasing half-cycles, respectively.

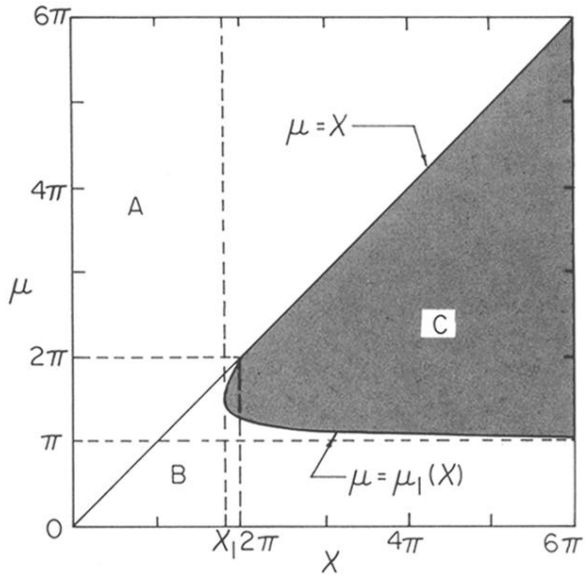

FIG. 1. Dissipation during constant rotation (a) is confined to within x_0 of either surface in region A, (b) occurs throughout the slab of thickness $X=2x_m$ in regions B and C, and (c) is unstable in region C (cross-hatched). Here, $\mu=k_{c\|}x_m$ and $\chi=k_{c\|}x_0$.